HDL-TR-2196

April 1991

Energy Levels and Branching Ratios of Tm^{3+} in Ten Garnet Laser Materials

by Clyde A. Morrison
Elizabeth D. Filer
Norman P. Barnes

U.S. Army Laboratory Command
Harry Diamond Laboratories
Adelphi, MD 20783-1197

REPORT DOCUMENTATION PAGE

Form Approved OMB No. 0704-0188

1. AGENCY USE ONLY *(Leave blank)*

2. REPORT DATE
April 1991

3. REPORT TYPE AND DATES COVERED
Interim, 15 June 1990 to 15 January 1991

4. TITLE AND SUBTITLE
Energy Levels and Branching Ratios of Tm^{3+} in Ten Garnet Laser Materials

5. FUNDING NUMBERS
DA PR: AH44
PE: 61102.H44

6. AUTHOR(S)
Clyde A. Morrison, HDL; Elizabeth D. Filer and Norman P. Barnes, NASA Langley

7. PERFORMING ORGANIZATION NAME(S) AND ADDRESS(ES)
Harry Diamond Laboratories
2800 Powder Mill Road
Adelphi, MD 20783-1197

8. PERFORMING ORGANIZATION REPORT NUMBER
HDL-TR-2196

9. SPONSORING/MONITORING AGENCY NAME(S) AND ADDRESS(ES)
NASA Langley Research Center
Hampton, VA 23665

10. SPONSORING/MONITORING AGENCY REPORT NUMBER

11. SUPPLEMENTARY NOTES
AMS code: 611102.H440011
HDL PR: 1AE151

12a. DISTRIBUTION/AVAILABILITY STATEMENT
Approved for public release; distribution unlimited.

12b. DISTRIBUTION CODE

13. ABSTRACT *(Maximum 200 words)*

A prediction of laser performance of Tm transitions from the $^3F_4$ to the $^3H_6$ manifolds in ten garnets has been made by using a quantum-mechanical model. Theoretical energy levels, branching ratios, and population inversion percentages were calculated to determine threshold as a function of temperature.

14. SUBJECT TERMS
Thulium, YAG, LaLuGG, GdScAG, YScAG, GdGG, GdScGG, YGG, LuGG, GdAG, LuAG, garnets

15. NUMBER OF PAGES
23

16. PRICE CODE

17. SECURITY CLASSIFICATION OF REPORT	18. SECURITY CLASSIFICATION OF THIS PAGE	17. SECURITY CLASSIFICATION OF ABSTRACT	20. LIMITATION OF ABSTRACT
Unclassified	Unclassified	Unclassified	UL

NSN 7540-01-280-5500

Standard Form 298 (Rev. 2-89)
Prescribed by ANSI Std. Z39-18
298-102

91 4 30 007

Contents

Figures

Tables

1. Introduction

In the search for solid-state lasers with wavelengths longer than 1.5 µm, thulium appears to be an important element for two reasons. One, thulium has been shown to lase at wavelengths slightly shorter than 2.0 µm [1]. Second, the thulium ion has an absorption band at about 0.78 µm [2]. Absorption bands in this region are amenable to laser diode pumping using GaAlAs laser technology. Coupled with the 2:1 quantum efficiency of this pump band, thulium has the potential to become an efficient laser. Thus, thulium may be the most practical long-wavelength laser.

However, in general, the $^3F_4$ to $^3H_6$ transitions have been found to be relatively weak, leading to small emission cross sections. To overcome this deficiency, a garnet material has been sought which has a large emission cross section. Another reason for studying thulium in garnets is its use as a sensitizer for a holmium laser. Holmium, with its tendency to have a larger emission cross section, may be a more efficient laser if it can be efficiently pumped. However, holmium lacks absorption bands in the spectral region amenable to GaAlAs technology. To overcome this deficiency, the garnet laser material could be sensitized with thulium, which will become the primary absorber of diode radiation. However, for efficient energy transfer to occur, a near coincidence of energy differences between the holmium and thulium manifolds should exist [3]. For either reason, the energy levels and the branching ratios of the $^3F_4$ to $^3H_6$ transitions must be known.

While many garnet materials can be grown, the required spectroscopic information on the thulium manifolds is, in general, not known for these materials. Even in $Y_3Al_5O_{12}$ the ground manifold has not been well determined for thulium since several levels have not been observed [2]. Although experimental measurements are desirable, the resources required to spectroscopically analyze all possible garnet materials are prohibitive. To circumvent this problem, a quantum mechanical model of lanthanide series elements can be used to indicate the most promising garnets. A quantum mechanical point charge model, developed at the Harry Diamond Laboratories [4], was used to calculate the energy levels and branching ratios of thulium. Required input for this model consists of the x-ray data and the refractive index as a function of wavelength. To provide the dispersion of the refractive index, we used a standard Sellmeier equation, obtained by fitting experimental refractive index values. From the required inputs, the model predicts both the energy levels and the dipole transition matrix elements. Both electric and magnetic dipole line strengths are calculated since in some cases both contributions are comparable. With the position of the energy levels and the dipole line strengths known, the gain of a potential garnet laser material can be estimated. Given a calculated gain, thresholds can, in turn, be predicted, and thus the laser potential of a particular garnet can be assessed. By comparing the laser threshold of all garnets, we can evaluate the efficacy of pursuing the growth of a particular garnet.

While numerous laser materials could be grown, the garnets were selected for initial evaluation based on their desirable properties. Among the desirable properties of the garnets is a relatively strong crystal field [5]. A strong crystal field is desirable to obtain a large splitting of the ground manifold. A large ground-state splitting promotes a lower population density in the lower laser level and thus a lower threshold. In addition, the garnets tend to have desirable thermal properties, especially the large thermal conductivity [6]. A large thermal conductivity, coupled with the good mechanical properties of garnets, allows the garnets to be used in high average power situations. Garnets are often relatively straightforward to grow, and they are durable enough to be fabricated into useful laser materials.

To evaluate the garnet laser materials, the threshold of the possible $^3F_4$ to $^3H_6$ transitions in Tm^{3+} in the various materials was calculated as a function of temperature. In order to achieve

threshold, the gain must exceed the loss. For a transition such as the $^3F_4$ to $^3H_6$ in thulium, a large thermal population exists in the lower laser level. An obvious reason for the large lower-laser-level population density is the proximity of the ground level. Thus, exceeding threshold requires that the population density of the upper laser level must exceed the thermal population density in the lower laser level. In addition, the population inversion density must be sufficiently high that the gain exceeds the losses in the laser resonator. To minimize threshold, a lower laser level should be sought which minimizes the thermal population density, and a transition should be sought which maximizes the transition probability. In essence, the latter implies that a transition with a high branching ratio should be sought. A figure of merit which includes both effects is established to evaluate the various garnet laser materials.

Reported here are the calculated energy levels, the branching ratios, and the estimated thresholds for thulium operating on the $^3F_4$ to $^3H_6$ transitions. Garnet materials, with the general formula $A_3B_2C_3O_{12}$, are evaluated. Calculations are done for the A site under the assumption of D_2 symmetry. X-ray data, available in the literature, are used to evaluate the crystal-field components, A_{nm}. Even-n components are then used to calculate the crystal-field splittings within the manifold. With a knowledge of the energy levels, we determine thermal occupation factors in a straightforward manner using a Boltzmann distribution for the respective manifolds. Odd-n components are used to calculate the transition probabilities for electric field transitions. It was determined that the magnetic dipole contributions to the transition probability are comparable to the electric dipole contributions in some cases. Consequently, both magnetic and electric dipole transition probabilities were used in the calculation of the branching ratios. Given the thermal occupation factors and the branching ratios, we calculate thresholds as a function of the density of thulium atoms. For these calculations, equal losses were assumed for all the various garnet laser materials.

2. Crystal-Field Calculations

The calculations performed here are similar to those given by Morrison et al [7]; consequently, a number of details will be omitted. For all the host materials considered, the free-ion parameters chosen were those of Carnall et al [8]. For triply ionized thulium ions in aqueous solution these parameters are:

$$\begin{aligned} &E^{(1)} = 7{,}142 \quad E^{(2)} = 33.795 \quad E^{(3)} = 674.27 \\ &\zeta = 2{,}628.7 \quad \alpha = 14.677 \quad \beta = -631.79 \\ &\gamma = 0\ \mathrm{cm}^{-1}\ . \end{aligned} \tag{1}$$

The crystal-field Hamiltonian appropriate for Tm^{3+} $(4f^{12})$ is of the form

$$H_{CEF} = \sum_{n,m} B^*_{nm} \sum_{i=1}^{12} C_{nm}(i) \quad , \tag{2}$$

where the nonvanishing B_{nm} appropriate for D_2 symmetry are all real [9]. The free-ion Hamiltonian, with the parameters given in equation (1) along with the crystal-field Hamiltonian in equation (2), has been used by Gruber et al [2] to analyze the optical spectrum of Tm^{3+} in $Y_3Al_5O_{12}$ (YAG). The resulting best fit crystal-field parameters obtained are as follows:

$$\begin{aligned} &B_{20} = 474 \quad B_{22} = 47.0 \quad B_{40} = -213 \\ &B_{42} = -1{,}571 \quad B_{44} = -824 \quad B_{60} = -984 \\ &B_{62} = -310 \quad B_{64} = 591 \quad B_{66} = -193\ \mathrm{cm}^{-1}\ . \end{aligned} \tag{3}$$

In the fitting procedure used by Gruber et al [2], the centroids of the LSJ multiplets were allowed to vary in the manner described by Morrison and Leavitt [10], and the resulting centroids of the multiplets of interest here are 456 cm^{-1} for the $^3H_6$ manifold and 5986 cm^{-1} for the $^3F_4$ manifold. Since we have no experimental data on the spectra of Tm^{3+} in the other garnets, we use these centroids in the remaining analysis (In fact, all the centroids reported by Gruber et al [2] were used). From previous analysis we have found that the branching ratios, crystal-field splitting within a multiplet, and electric and magnetic dipole line strengths are not sensitive to reasonable variations of the cen-

troids [10]. Nevertheless, it must be kept in mind that the wavelengths calculated for the $^3F_4$ to $^3H_6$ transitions are only approximations.

Using the crystal-field parameters, B_{nm}, given in equation (3) and the crystal-field components, A_{nm}, for YAG with the oxygen charge, q_o, equal to −1.7 from Morrison et al [7], we calculate the rotational invariants $S_n(B)$ and $S_n(A)$. Assuming that the calculated crystal-field parameters are given by

$$B_{nm} = \rho_n A_{nm} \quad , \qquad (4)$$

we obtain

$$\begin{aligned} \rho_2 &= 0.08583\ (\text{Å}^2) \\ \rho_4 &= 0.2956\ (\text{Å}^4) \\ \rho_6 &= 0.6384\ (\text{Å}^6) \quad , \end{aligned} \qquad (5)$$

by using equation (8) of reference 7. The crystal-field parameters for even-n values were calculated for each of the garnets with the use of equations (4) and (5). Values of A_{nm} for $q_o = -1.7$ are from Morrison et al [7], and the results are given in table 1. As in reference 7, the value of the B_{20} and B_{22} are significantly different for the two choices of reported x-ray data for YScAG. These differences indicate the accuracy needed in the x-ray data. B_{20} and B_{22} are more sensitive to the lattice sums since more ions are covered for A_{2m} than for A_{4m} and A_{6m}, so that all sums have the same number of significant digits.

The odd-n A_{nm} for $q_o = -1.7$ from Morrison et al [7] were used to calculate the Judd-Ofelt parameters given in table 2. Three sets of these parameters have been reported for Tm^{3+}:YAG [9]. A comparison shows the Ω_2 approximately an order of magnitude less than the experimental values while Ω_4 approximately equals the experimental values, and the calculated Ω_6 is approximately five times too large. Judd-Ofelt parameters are not applicable here because of the relatively large contributions from the magnetic dipole transition for the $^3F_4$ to $^3H_6$ transitions.

Using the B_{nm} of table 1, we calculated the energy levels of Tm^{3+} for each of the garnets, with the results given in table 3. The values for the energy levels of the $^3H_6$ multiplet of Tm^{3+} in YAG obtained by using the best-fit B_{nm} of Gruber et al [2] differ somewhat from the corresponding energy levels obtained by using the B_{nm} of table 1. However, experimental energy levels are missing and levels 5 and 6 are reversed. Further experimental work is needed on this multiplet. The irreducible representations (IR's) of the ground state and the first excited state remain the same for all the garnets. This result is important in the analysis of the experimental absorption data taken at low temperature since it serves as a means of identifying the IR of the excited levels ($\Gamma_i \rightarrow \Gamma_i$ transitions are forbidden for both electric and magnetic dipoles). The IR's of the higher energy levels of the $^3H_6$ multiplet are quite sensitive to the values of B_{nm}, and as can be seen, vary considerably for the different garnets. A wide variation in the higher levels of the $^3H_6$ multiplet is of considerable interest since these levels are most likely to be involved in the lasing process as the lower laser level. In the $^3F_4$ multiplet, only two levels, numbers 20 and 21, have different IR's for the various garnets in table 3.

3. Branching Ratios

The details of calculating the branching ratios have been given by Morrison et al [7], and we refer the reader to that reference for the details. The odd-n A_{nm} used in the calculations of the electric dipole line strengths, S_{ij}^{ed}, are from table 6 of that reference. The branching ratio for the transition of level i of the $^3F_4$ ($i = 14 \rightarrow 22$, table 3) to the level j of $^3H_6$ ($j = 1 \rightarrow 13$, table 3) is given by

$$\beta_{ij}(T) = \frac{\dfrac{Z_i}{\tau_{ij}}}{\displaystyle\sum_{ij} \frac{Z_i}{\tau_{ij}}} \quad , \qquad (6)$$

with

$$Z_i = \frac{\exp(-E_i/kT)}{\displaystyle\sum_i \exp(-E_i/kT)} \quad . \qquad (7)$$

Table 1. Theoretical crystal-field parameters, B_{nm}(cm^{-1}), for Tm^{3+} in garnets

B_{nm}	1 YAG	2 LaLuGG	3 GdScAG	4 YScAG(1)	5 YScAG(2)	6 GdGG
B_{20}	373	313	483	440	316	101
B_{22}	212	115	231	191	6.44	85.7
B_{40}	–68.0	–5.53	25.9	11.5	–86.0	–73.6
B_{42}	–1591	–1270	–1473	–1580	–1709	–1456
B_{44}	–797	–597	–667	–727	–821	–780
B_{60}	–1026	–626	–827	–885	–949	–850
B_{62}	–398	–303	–392	–423	–445	–311
B_{64}	398	313	363	410	479	393
B_{66}	–352	–260	–323	–354	–359	–317

B_{nm}	7 GdScGG	8 YGG	9 LuGG	10 GdAG	11 LuAG
B_{20}	240	65.8	9.44	319	278
B_{22}	89.0	21.4	–95.3	237	146
B_{40}	–41.1	–101	–155	–56.8	–74.2
B_{42}	–1423	–1563	–1700	–1484	–1748
B_{44}	–705	–843	–925	–758	–889
B_{60}	–772	–915	–991	–949	–1108
B_{62}	–333	–338	–372	–351	–435
B_{64}	372	443	512	363	482
B_{66}	–300	–338	–356	–331	–401

Table 2. Theoretical Judd-Ofelt parameters ($\times 10^{-20}$ cm^2) for Tm^{3+} in garnets

Compound	Ω_2	Ω_4	Ω_6
YAG	0.06568	0.6760	3.764
LaLuGG	0.09924	0.4384	1.716
GdScAG	0.03742	0.4752	2.742
YScAG(1)	0.07334	0.5930	3.091
YScAG(2)	0.07245	0.6450	3.467
GdGG	0.01498	0.4184	2.654
GdScGG	0.01695	0.3811	2.370
YGG	0.008409	0.4622	3.041
LuGG	0.002876	0.5246	3.547
GdAG	0.08354	0.6300	3.224
LuAG	0.01580	0.6607	4.296

Table 3. Energy levels (cm^{-1}) of the $^3H_6$ and $^3F_4$ multiplets of Tm^{3+}

No.[a]	YAG[b]		YAG[c]		LaLuGG		GdScAG		YScAG(1)		YScAG(2)		GdGG		GdScGG		YGG		LuGG		GdAG		LuAG	
	IR[d]	E	IR	E	IR	E	IR	E	IR	E	IR	E	IR	E	IR	E	IR	E	IR	E	IR	E	IR	E
1	2	0	2	0	2	0	2	0	2	0	2	0	2	0	2	0	2	0	2	0	2	0	2	0
2	1	27	1	13	1	10	1	9	1	13	1	36	1	26	1	18	1	43	1	83	1	11	1	25
3	4	218	2	278	2	186	2	289	2	268	3	172	4	151	3	177	4	127	4	97	2	270	4	239
4	3	228	4	285	3	188	3	297	3	272	4	183	3	159	2	178	3	133	3	100	4	278	2	244
5	1	256	3	295	4	200	4	312	4	287	2	197	2	164	4	180	2	160	1	145	3	292	3	247
6	2	266	1	354	1	237	1	368	1	347	1	237	1	199	1	226	1	176	2	179	1	344	1	312
7	4	520	4	600	4	443	4	555	4	578	4	552	4	512	4	490	4	528	4	545	4	575	4	630
8	3	613	3	660	3	479	3	601	3	633	1	643	3	543	3	537	3	560	1	580	3	617	3	705
9	1	652	2	701	1	515	2	657	2	678	3	645	1	553	1	557	1	565	3	583	2	661	2	729
10	2	687	1	708	2	522	1	668	1	688	2	675	3	574	2	570	2	607	2	654	1	676	1	729
11	4	701	4	731	4	538	4	687	4	710	3	705	2	578	3	587	3	616	3	686	4	689	3	743
12	3	754	3	740	3	559	3	736	3	741	4	712	4	601	4	591	4	639	1	686	3	690	4	767
13	1	767	1	762	1	576	1	750	1	759	1	729	1	610	1	612	1	640	4	704	1	711	1	777
14	1	5539	1	5571	1	5545	1	5597	1	5570	1	5497	1	5498	1	5518	1	5477	1	5458	1	5577	1	5526
15	3	5760	3	5796	3	5717	3	5795	3	5787	3	5735	3	5719	3	5720	3	5716	3	5718	3	5790	3	5783
16	2	5813	2	5864	2	5766	2	5870	2	5861	2	5799	2	5753	2	5767	2	5749	2	5749	2	5849	2	5846
17	4	5915	4	5933	4	5817	4	5925	4	5924	4	5889	4	5816	4	5830	4	5822	4	5840	4	5908	4	5924
18	1	6043	1	6076	1	5919	1	6061	1	6070	1	6026	1	5941	1	5947	1	5955	1	5978	1	6042	1	6089
19	2	6114	2	6149	2	5967	2	6101	2	6120	2	6110	2	6024	2	6014	2	6050	2	6092	2	6112	2	6173
20	1	6166	4	6241	4	6057	4	6196	4	6215	4	6203	1	6106	4	6107	1	6130	1	6166	1	6202	1	6266
21	4	6231	1	6243	1	6065	1	6214	1	6233	1	6208	4	6119	1	6107	4	6147	4	6191	4	6205	4	6269
22	3	6246	3	6261	3	6080	3	6224	3	6248	3	6241	3	6132	3	6128	3	6163	3	6213	3	6218	3	6294

[a]*This number is used for referral in the text and figures.*
[b]*Best fit B_{nm} (Gruber et al [2]).*
[c]*B_{nm} from table 1.*
[d]*Irreducible representations of the D_2 group.*

In this expression τ_{ij} is the inverse of the transition rate between the i and j levels, and can be calculated as

$$\frac{1}{\tau_{ij}} = \frac{32\pi^3\alpha}{3c^2}\left(X_{ij}\, S_{ij}^{ed} + X_{ij}^{'}\, S_{ij}^{md}\right) \nu_{ij}^3 , \quad (8)$$

with

$$X_{ij} = \frac{n_{ij}\left(n_{ij}^2 + 2\right)^2}{9} , \quad (9)$$

and

$$X_{ij}^{'} = n_{ij}^3 \ . \quad (10)$$

Here n_{ij} is the index of refraction at wavelength λ_{ij}, and α is the fine structure constant. The temperature dependence of the branching ratio enters through the Boltzmann factor given in equation (7). Dispersion in the index of refraction is taken into account by use of a Sellmeier equation,

$$n^2 = A + B\lambda^2 / \left(\lambda^2 - C\right) + D\lambda^2 / \left(\lambda^2 - E\right), \quad (11)$$

with the constants given in table 7 of reference 7. The three highest branching ratios for the $^3F_4$ to $^3H_6$ were calculated for the temperature range 50 K < T < 400 K, and the results are given in figures 1 and 2.

4. Laser Threshold

A detailed discussion of the equations governing the calculation of laser threshold and the approximations made in their derivation is given by Morrison et al [7]. Only the pertinent equations will be given here. The figure of merit is the ratio of the number of ions in the $^3F_4$ multiplet (N_2) to the total number of thulium ions (N_A) at threshold; that is

$$\frac{N_2}{N_A} = \frac{\dfrac{Z_j}{Z_i + Z_j} + G_{ij} + \sum_{km}{}' H_{ij}^{km}}{1 + \sum_{km}{}' F_{ij}^{km}} \ . \quad (12)$$

We shall refer to the best figure of merit as those transitions which have the lowest N_2/N_A ratio. The i to j transition is assumed to be the laser transition, $\nu_{ij} = \nu_o$, in a normalized Lorentzian line shape $g(\nu)$. The sums on k and m in equation (12) are such that $k \neq i$ and $m \neq j$ simultaneously. These sums are further restricted here by the choice

$$E_k - E_m = E_i - E_j \pm \Delta E \ . \quad (13)$$

The factors entering equation (12) are

$$G_{ij} = \frac{-\ln\left(R_m R_L\right) 4\pi^2 \Delta\nu\ n_{ij}^2 \tau_{ij}}{2l N_A \left(Z_i + Z_j\right) \lambda_{ij}^2} ,$$

$$H_{ij}^{km} = \frac{\pi\Delta\nu}{2} \frac{g(\nu_{km})\ \tau_{ij} Z_m}{\tau_{km}\left(Z_i + Z_j\right)} , \quad (14)$$

$$F_{ij}^{km} = \frac{\pi\Delta\nu}{2} \frac{g(\nu_{km}) \left(Z_k + Z_m\right)\tau_{ij}}{\left(Z_i + Z_j\right)\tau_{km}} ,$$

and Z_i and Z_j are the Boltzmann factors for the $^3F_4$ and $^3H_6$ manifolds, respectively. Equations (13) and (14) were used in equation (12) to determine the threshold conditions for Tm^{3+} in the various garnets.

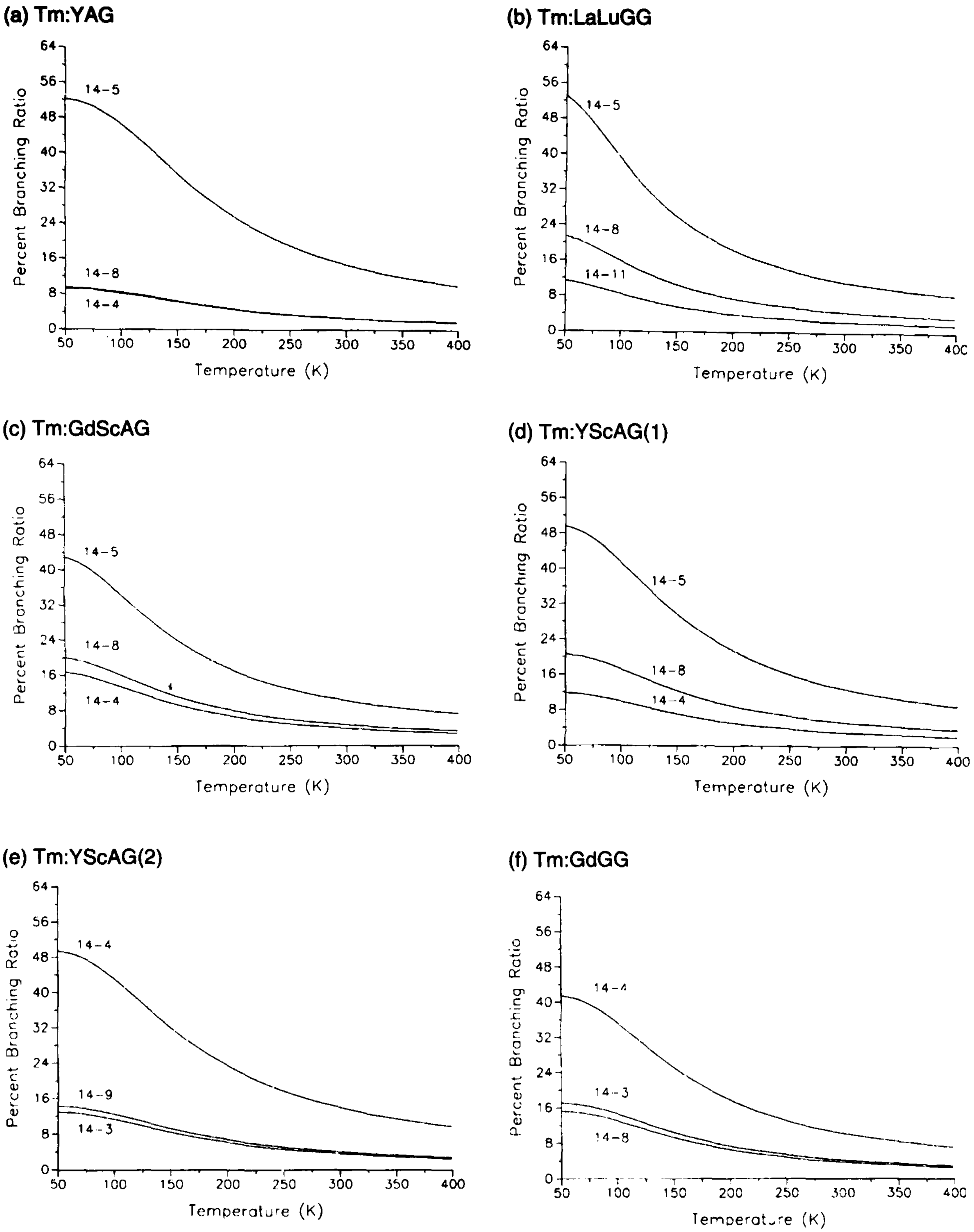

Figure 1. Branching ratio as a function of temperature for Tm^{3+} in YAG, LaLuGG, GdScAG, YScAG(1), YScAG(2), and GdGG.

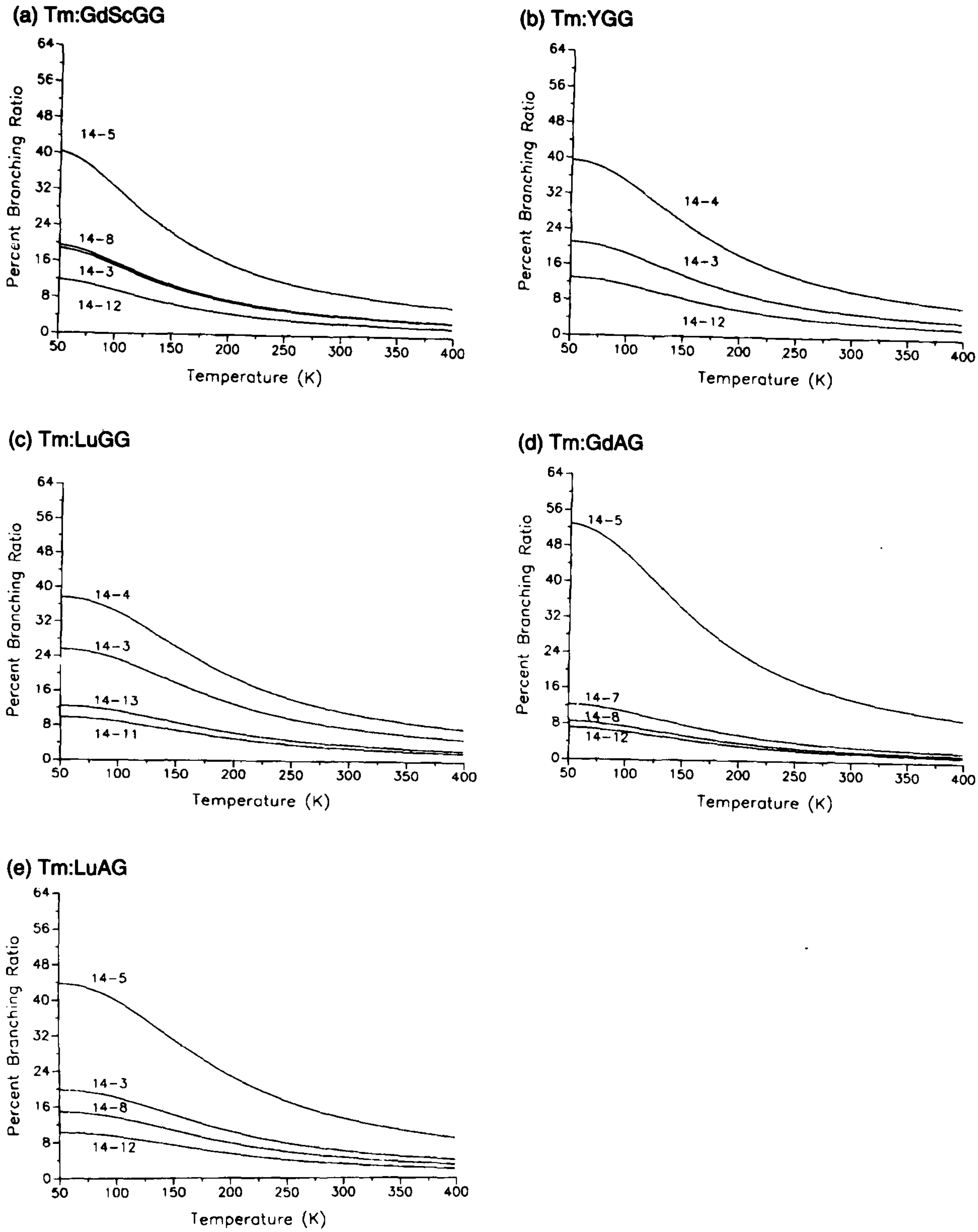

Figure 2. Branching ratio as a function of temperature for Tm^{3+} in GdScGG, YGG, LuGG, GdAG, and LuAG.

5. Results and Discussion

To evaluate the best choices of materials for a thulium laser, we determine theoretical branching ratios for all the $^3F_4$ to $^3H_6$ levels of Tm^{3+} in the ten garnets, for a temperature range between 50 and 400 K. As shown in figures 1 and 2, we used the transitions with the highest branching ratios at 75 K as the basis for the figure-of-merit plots. This was because we have empirically determined that the best figure of merit (lowest population inversion required for threshold) is found from among those transitions with the highest branching ratios at low temperatures for a given material. This is in contrast to holmium in garnets, where it was observed that the best figure-of-merit line came from lines having the top three or four branching ratios at room temperature, 300 K. The transition with the best figure of merit for each material for thulium had the lowest level (level number 14) in the upper manifold as the upper laser level.

Some reasonable values of the parameters of the laser system are needed in determining the figure of merit. If different values were assumed for rod length, l, reflectivity of the output mirror, R_m, reflectivity representing other losses in the resonator, R_L, and concentration of the thulium, for example, then the lines would be shifted relative to each other on the figure-of-merit plots. We assumed a concentration of the thulium of 0.8 percent, reflectivity of the output mirror of 80 percent, reflectivity representing other losses in the resonator at 90 percent, and rod length of 0.05 m. Other lines may have been close enough to contribute to the center line when the laser threshold was determined. The criteria determining that a line was contributing were that the line needed to have an energy difference (ΔE in eq (13)) within 3 cm^{-1} of the principal line and a branching ratio at least 10 percent as large as the principal line. In holmium the energy levels were close together, and contributions to the principal line occurred frequently. We did not find this to be true for thulium.

In GdScGG, the 14→3 line contributed to the 14→5 figure of merit, and the 14→11 line contributed to the 14→12 line. In LuGG, the 14→3 contributed to the 14→4 transition. But no other contributions were made among any of the top three branching ratio transitions used for finding laser thresholds. As can be seen in the figure-of-merit plots, figures 3 and 4, two lines of LuAG had the lowest thresholds at room temperature out of all ten garnets. LuAG seems to be a very promising laser material for thulium. At 75 K, YAG had the best figure of merit. A summary of each of the garnets appears below. Overall, aluminum garnets seemed to be preferred over gallium garnets both at high and low temperatures.

YAG

For YAG, the 14→5 (1.895 μm) transition had the highest branching ratio at 75 K, followed by the 14→8 (2.036 μm) and 14→4 (1.892 μm) transitions. Up to 100 K, the 14→5 line had the lowest figure of merit as well. There was a crossover, and over 125 K the 14→8 line had the best figure of merit. Actually, it is known experimentally that the 14→5 transition is 1.884 μm, with the 14→4 at 1.882 μm [2]. Our theoretical predictions were too high by about 0.01 μm on these two lines. Nevertheless, the laser thresholds found from the figure-of-merit calculations were as expected, since from experiment it is known that the lasing line at low temperature is at 1.88 μm, but at room temperature the 2.01-μm line is observed to lase [11]. The figure-of-merit plot for YAG indicated the same preference for lasing as a function of temperature, even though the actual magnitude of the wavelengths was not exact. Correlation of experimental data with the figure-of-merit calculations greatly increases the confidence in the model, especially for YAG. For the other garnets, no experimental data were available as a check on the laser threshold predictions. Out of all the garnets considered the 14→5 line of YAG was found to have the best figure of merit at 75 K.

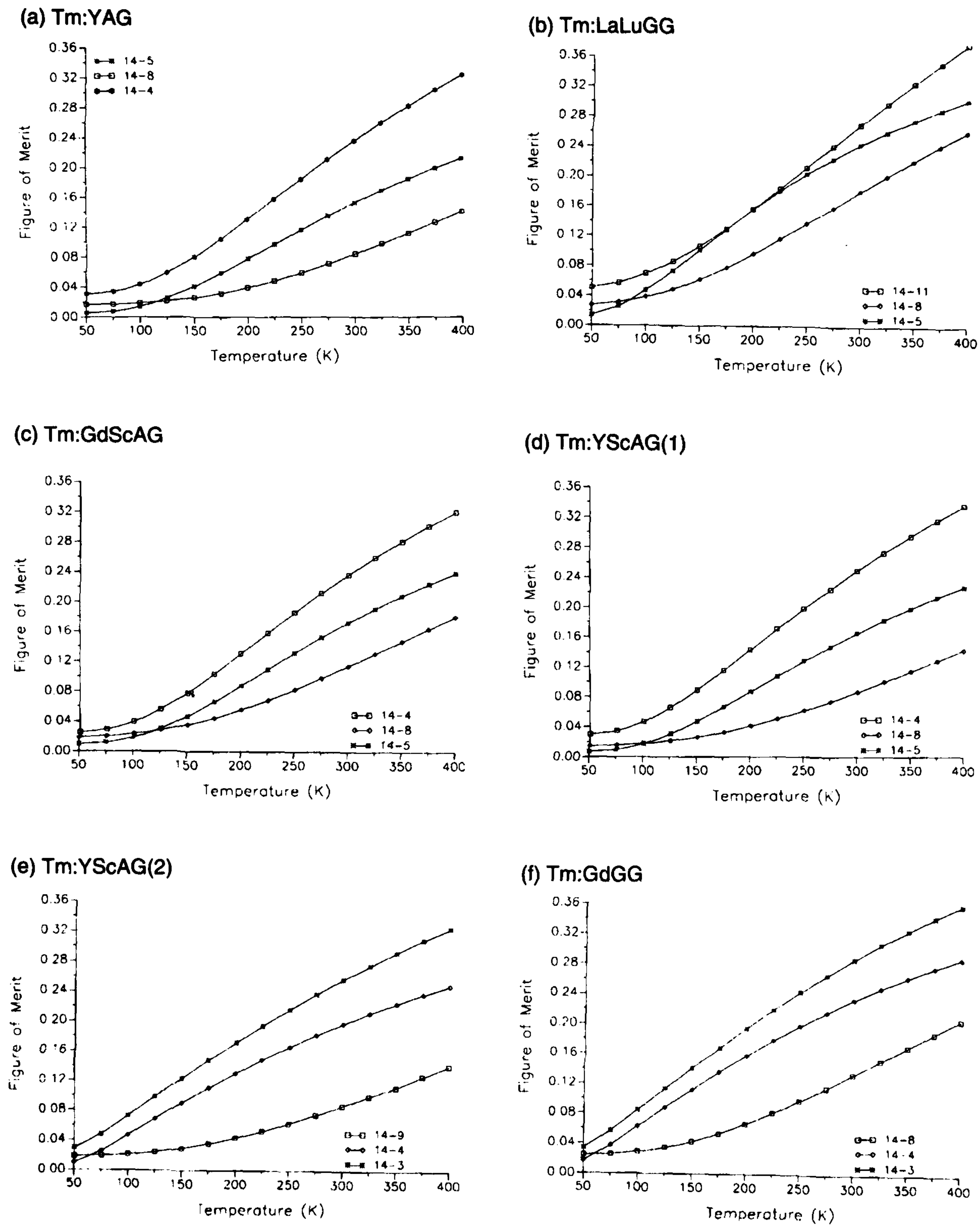

Figure 3. Figure of merit as a function of temperature for Tm^{3+} in YAG, LaLuGG, GdScAG, YScAG(1), YScAG(2), and GdGG.

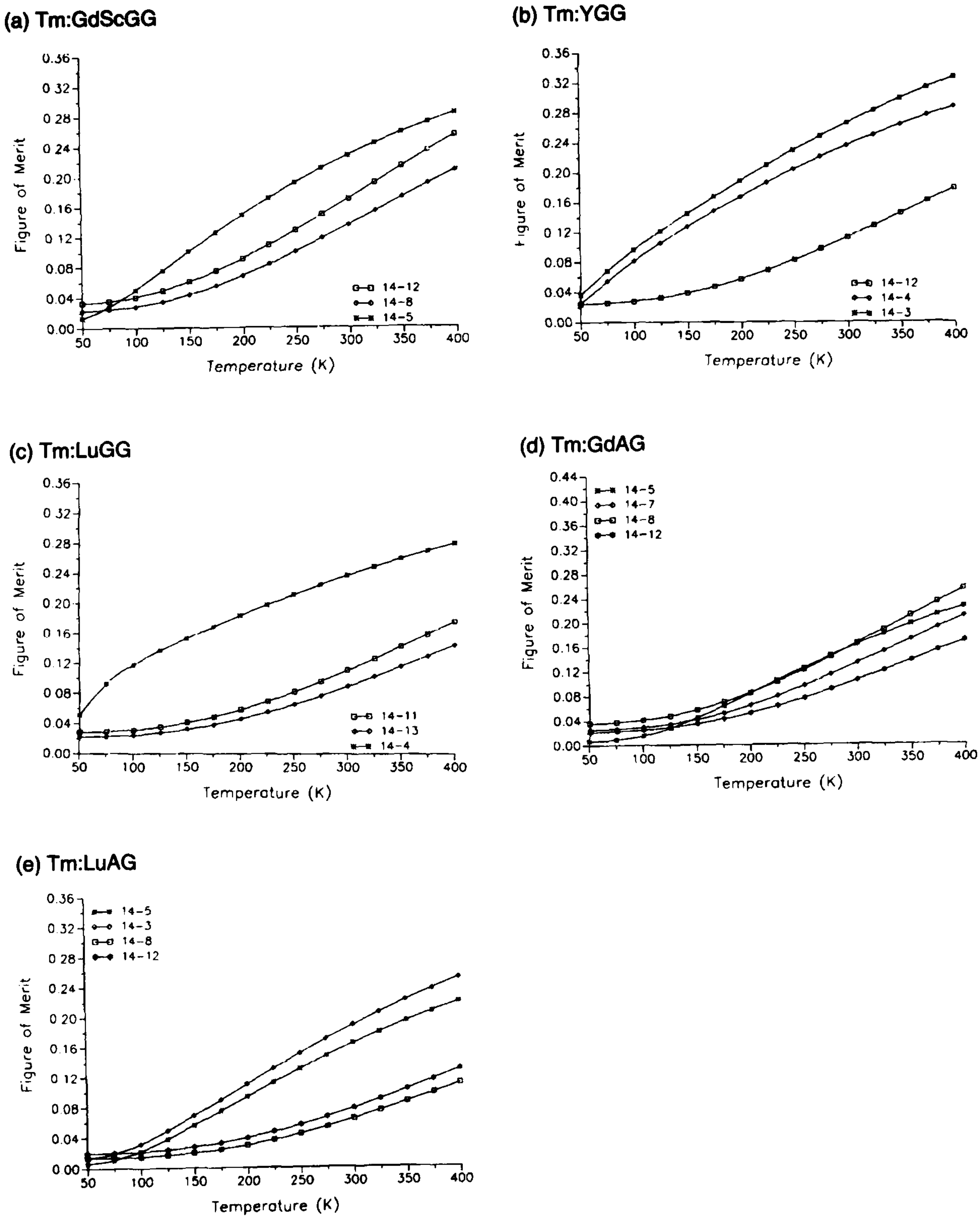

Figure 4. Figure of merit as a function of temperature for Tm^{3+} in GdScGG, YGG, LuGG, GdAG, and LuAG.

LaLuGG

The 14→5 (1.871 μm) transition of LaLuGG had the highest branching ratio at 75 K, followed by the 14→8 (1.974 μm) line and the 14→11 (1.997 μm) line. At 75 K and below, the 14→5 line had the best figure of merit also. But at 100 K and up, the 14→8 line is the best. LaLuGG was unique in that it had the largest manifold lifetime out of all the hosts considered. It also had the smallest splitting of the lower manifold. Because of these properties, LaLuGG does not seem to be a promising material.

GdScAG

GdScAG also had the 14→5 (1.892 μm) transition with the highest branching ratio at 75 K, followed by the 14→8 (2.001 μm) and 14→4 (1.887 μm) lines. For 100 K and below, the 14→5 line had the best figure of merit. The 14→8 line was the best for temperatures at 125 K and above.

YScAG(1)

For YScAG(1), the 14→5 (1.893 μm) line had the highest branching ratio at 75 K, followed by the 14→8 (2.026 μm) and 14→4 (1.888 μm) lines. Up to 100 K the 14→5 line also has the best figure of merit, with 14→8 best above this temperature. YScAG(l) (the 14→5 line) ranked as the material with the third best laser threshold at 75 K. At room temperature it was the material with the fourth best figure of merit. YScAG(l), LuAG, and YAG all ranked within the five best materials for the figure of merit at both room temperature and 75 K.

YScAG(2)

Because we had two different sets of x-ray data, we determined branching ratios based on both. For YScAG(2), the 14→4 (1.882 μm) transition had the highest branching ratio at 75 K, followed by the 14→9 (2.061 μm) and 14→3 (1.878 μm) lines. The 14→4 transition had the best figure of merit at 50 K, but the 14→9 was best from 75 K and above. In YScAG(2), the third energy level in the lower manifold had a Γ_3 irreducible representation. Level 4 was a Γ_4, and level 9 was a Γ_3 irreducible representation. But the irreducible representations were flipped in YScAG(1), with level 4 being a Γ_3; level 5, a Γ_4; and level 8, a Γ_3. This flipping of the irreducible representations may account for the displacement of the lower laser level by one in the different sets of YScAG data. The different sets of x-ray data resulted in differences in energy level and transition probability predictions.

GdGG

For GdGG, the 14→4 (1.873 μm) line was the highest branching ratio, with the 14→3 (1.870 μm) and 14→8 (2.018 μm) lines next. The 14→4 had the best figure of merit at 50 K. At 75 K and above, however, the 14→8 was the best figure of merit. This material, and also the following three gallium garnets, had higher laser thresholds than each of their aluminum garnet counterparts, and so would make less desirable laser hosts for thulium.

GdScGG

For GdScGG, the 14→5 (1.873 μm) line had the highest branching ratio at 75 K, with the 14→8 (2.008 μm), 14→3 (1.872 μm), and 14→12 (2.030 μm) lines following. The 14→5 transition had the best figure of merit at 50 K, but the 14→8 line is best above 75 K. The 14→3 line contributed to the 14→5 figure of merit as mentioned before, and the 14→11 line contributed to the 14→12 line since the energy difference was within 5 cm^{-1}.

YGG

For YGG, the top branching ratio lines at 75 K were the 14→4 (1.871 μm), the 14→3 (1.869 μm), and the 14→12 (2.067 μm) transitions. A near coincidence of these first two lines may

produce an overlap effect which enhances the lasing on this transition, even though the lines are slightly farther apart than 5 cm^{-1}. The 14→12 line had the best figure of merit at all temperatures for YGG.

LuGG

For LuGG, the top branching ratios at 75 K were the 14→4 (1.867 μm), 14→3 (1.865 μm), 14→13 (2.104 μm), and 14→11 (2.096 μm) transitions. The 14→13 had the best figure of merit at all temperatures. For LuGG, the 14→3 line contributed to the 14→4 line. LuGG was the most promising of all the gallium garnet hosts. It had lower thresholds than the other gallium garnets at both 75 and 300 K.

GdAG

For GdAG, the 14→5 (1.892 μm) line was by far the highest branching ratio, followed by the 14→7 (1.999 μm), 14→8 (2.016 μm), and 14→12 (2.046 μm) lines at 75 K. At 125 K and below, the 14→5 transition had the best figure of merit, while the 14→12 was best at higher temperatures. GdAG (the 14→5 line) had the second best figure of merit at 75 K out of all ten garnets, with only YAG surpassing it.

LuAG

For LuAG, the highest branching ratio at 75 K was the 14→5 (1.894 μm) line. This was followed by the 14→3 (1.891 μm), 14→8 (2.074 μm), and 14→12 (2.101 μm) lines. The 14→5 had the best figure of merit at 75 K and below, but the 14→8 was best at 100 K and above. The 14→12 transition also had a very low figure of merit at room temperature, though not as good as the 14→8. The 14→8 transition and the 14→12 line were the two lines with the lowest laser threshold at room temperature out of all of the garnets we investigated. At room temperature, the figure of merit of LuAG was 0.064 for the 14→8 line, and 0.078 for the 14→12 line. LuAG surpassed YAG (the 14→8 of YAG was 0.084) in having a lower laser threshold at 300 K.

Finally, when the lowest laser thresholds of all the garnets are compared, at 75 K the 14→5 lines of YAG, GdAG, YScAG(1), LuAG, and GScAG were lowest. Likewise at room temperature, aluminum garnets were preferred. The lowest figure-of-merit lines at 300 K were, respectively, LuAG, the 14→8 line; LuAG, the 14→12 line; YAG, the 14→8 line; YScAG(1), the 14→8 line; and YScAG(2), the 14→9 line. LuAG seems to be the most promising laser host for room temperature. At low temperatures YAG was the preferred host.

References

[1] A. A. Kaminskii, *Laser Crystals*, Springer-Verlag, New York (1981), Chapter 5.

[2] J. B. Gruber, M. E. Hills, R. M. Macfarlane, C. A. Morrison, G. A. Turner, G. J. Quarles, G. J. Kintz, and L. Esterowitz, *Spectra and Energy Levels of* $Tm^{3+}:Y_3Al_5O_{12}$, Phys. Rev. **B40** (1989), 9464.

[3] D. L. Dexter, *A Theory of Sensitized Luminescence in Solids*, J. Chem. Phys. **21** (1953), 836. See also T. Y. Fan, G. Huber, R. L. Byer, and P. Mitzcherlich, *Spectroscopy and Diode Laser-Pumped Operation of Tm, Ho:YAG*, IEEE J. Quantum Electron., **24** (1988), 924. (The $^3H_4$ manifold in this paper corresponds to our $^3F_4$ manifold.)

[4] C. A. Morrison, N. Karayianis, and D. E. Wortman, *Rare-Earth Ion Host Lattice Interactions: 4. Predicting Spectra and Intensities of Lanthanides in Crystals*, Harry Diamond Laboratories, HDL-TR-1816 (1977).

[5] R. P. Leavitt, *On the Role of Certain Rotational Invariants in Crystal-Field Theory*, J. Chem. Phys. 77 (1982), 1661.

[6] V. F. Kitaeva, E. V. Zharikov, and I. L. Chistyi, *The Properties of Crystals with Garnet Structure*, Phys. Stat. Sol. **(a)92** (1985), 475.

[7] C. A. Morrison, E. D. Filer, N. P. Barnes, and G. A. Turner, *Theoretical Temperature Dependent Branching Ratios and Laser Thresholds of the* $^5I_7 \rightarrow {}^5I_8$ *Levels of* Ho^{3+} *in Ten Garnets*, Harry Diamond Laboratories, HDL-TR-2185 (1990).

[8] W. T. Carnall, P. R. Fields, and K. Rajnak, *Electronic Energy Levels in the Trivalent Lanthanide Aquo Ions: I. Pr^{3+}, Nd^{3+}, Pm^{3+}, Sm^{3+}, Dy^{3+}, Ho^{3+}, Er^{3+}, and Tm^{3+}*, J. Chem. Phys. **49** (1968), 4424.

[9] C. A. Morrison and R. P. Leavitt, in *Handbook on the Physics and Chemistry of Rare Earths V*, edited by K. A. Geschneidner, Jr., and L. Eyring, North Holland, NY (1982).

[10] C. A. Morrison and R. P. Leavitt, *Crystal-Field Analysis of Triply Ionized Rare Earth Ions in Lanthanum Trifluoride*, J. Chem. Phys. **71** (1979), 2366.

[11] N. P. Barnes and D. J. Gettemy, *Tm:YAG Lasers and Second Harmonic Generation*, presented at Conference on Laser Electro-Optics 83 (CLEO '83), Baltimore, MD, 17–20 May 1983.

DISTRIBUTION

Administrator
Defense Technical Information Center
Attn DTIC-DDA (2 copies)
Cameron Station, Building 5
Alexandria, VA 22304-6145

Director
Night Vision & Electro-Optics Laboratory
Attn Technical Library
Attn R. Buser
Attn A. Pinto
Attn J. Hebersat
Attn R. Rhode
Attn W. Tressel
Ft Belvoir, VA 22060

Director
Defense Advanced Research Projects Agency
Attn J. Friebele
1400 Wilson Blvd
Arlington, VA 22290

Director
Defense Nuclear Agency
Attn Tech Library
Washington, DC 20305

Under Secretary of Defense Res & Engineering
Attn Technical Library, 3C128
Washington, DC 20301

Office of the Deputy Chief of Staff for
Research, Development, & Acquisition
Department of the Army
Attn DAMA-ARZ-B, I. R. Hershner
Washington, DC 20310

Commander
US ArmyArmament Munitions & Chemical
Command (AMCCOM) R&D Center
Attn DRDAR-TSS, STINFO Div
Dover, NJ 07801

Commander
Atmospheric Sciences Laboratory
Attn Technical Library
White Sands Missile Range, NM 88002

Director
US Army Ballistics Research Laboratory
Attn SLCBR-DD-T (STINFO)
Aberdeen Proving Ground, MD 21005

Director
US Army Electronics Warfare Laboratory
Attn AMSEL-DD, J. Charlton
Ft Monmouth, NJ 07703

Commanding Officer
USA Foreign Science & Technology Center
Attn AIAST-BS, Basic Science Div
Federal Office Building
Charlottesville, VA 22901

Commander
US Army Materials & Mechanics Research
Center
Attn SLCMT-TL, Tech Library
Watertown, MA 02172

Director
US Army Materiel Systems Analysis Activity
Attn AMXSY-MP, Library
Aberdeen Proving Ground, MD 21005

Commander
US Army Missile & Munitions Center & School
Attn ATSK-CTD-F
Attn AMSMI-TB, Redstone Sci Info Center
Redstone Arsenal, AL 35809

Commander
US Army Research Office Durham
Attn R. J. Lontz
Attn M. Stosio
Attn M. Ciftan
Attn R. Guenther
Attn C. Bogosian
Research Triangle Park, NC 27709

Commander
USA Rsch & Std Gp (Europe)
Attn Chief, Physics & Math Branch
FPO, New York 09510

DISTRIBUTION (cont'd)

Commander
US Army Test & Evaluation Command
Attn D. H. Sliney
Attn Tech Library
Aberdeen Proving Ground, MD 21005

Commander
US Army Troop Support Command
Attn STRNC-RTL, Tech Library
Natick, MA 01762

Director
Naval Research Laboratory
Attn Code 2620, Tech Library Br
Attn G. Quarles
Attn G. Kintz
Attn A. Rosenbaum
Attn G. Risenblatt
Attn Code 5554, F. Bartoli
Attn Code 6540, S. R. Bowman
Attn Code 5554, L. Esterowitz
Attn Code 5554, R. E. Allen
Washington, DC 20375

Commander
Naval Weapons Center
Attn Code 3854, R. Schwartz
Attn Code 3854, M. Hills
Attn Code 3854, M. Nadler
Attn Code 3854, R. L. Atkins
Attn DOCE 343, Technical Information Department
China Lake, CA 93555

Air Force Office of Scientific Research
Attn Major H. V. Winsor, USAF
Bolling AFB
Washington, DC 20332

Department of Commerce
National Institute of Science and Technology
Attn Library
Washington, DC 20234

NASA Langley Research Center
Attn N. P. Barnes (20 copies)
Attn G. Armagan
Attn F. Allario
Attn P. Cross
Attn N. Y. Chou
Attn J. Barnes

NASA Langley Research Center (cont'd)
Attn E. Filer (10 copies)
Attn C. Bair
Attn M. Buoncristiani
Hampton, VA 23665

Director
Advisory Group on Electron Devices
Attn Sectry, Working Group D
201 Varick Street
New York, NY 10013

Aerospace Corporation
Attn M. Birnbaum
Attn N. C. Chang
Attn T. S. Rose
PO Box 92957
Los Angeles, CA 90009

Allied Signal Inc
Advanced Application Dept
Attn A. Budgor
31717 La Tiemda Drive
Westlake Village, CA 91362

Allied Signal Inc
Attn Y. Band
Attn R. Morris
POB 1021R
Morristown, NJ 07960

Ames Laboratory Dow
Iowa State University
Attn K. A. Gschneidner, Jr. (2 copies)
Ames, IA 50011

Argonne National Laboratory
Attn W. T. Carnall
9700 South Cass Avenue
Argonne, IL 60439

Booz, Allen and Hamilton
Attn W. Drozdoski
4330 East West Highway
Bethesda, MD 20814

Draper Lab
Attn F. Hakimi
MS 53555 Tech Sq
Cambridge, MA 02139

DISTRIBUTION (cont'd)

Engineering Societies Library
Attn Acquisitions Dept
345 E. 47th Street
New York, NY 10017

Fibertech, Inc.
Attn H. R. Verdin (3 copies)
510-A Herdon Pkwy
Herdon, VA 22070

General Dynamics
Attn R. J. Blair
5452 Oberlin Drive
San Diego, CA 92121

Hughes Aircraft Company
Attn D. Sumida
3011 Malibu Canyon Rd
Malibu, CA 90265

IBM Research Division
Almaden Research Center
Attn R. M. Macfarlane, Mail Stop K32 802(d)
650 Harry Road
San Jose, CA 95120

Director
Lawrence Radiation Laboratory
Attn M. J. Weber
Attn H. A. Koehler
Attn W. Krupke
Livermore, CA 94550

LTV
Attn M. Kock (WT-50)
PO Box 650003
Dallas, TX 75265

Martin Marietta
Attn F. Crowne
Attn J. Little
Attn T. Worchesky
1450 South Rolling Road
Baltimore, MD 21227

McDonnell Douglass Electronic Systems
Company
Dept Y440, Bldg. 101, Lev. 2 Rm/Pt B54
Attn D. M. Andrauskas, MS-2066267
PO Box 516
St Louis, MO 63166

MIT Lincoln Lab
Attn B. Aull
PO Box 73
Lexington, MA 02173

Department of Mechanical, Industrial, & Aerospace Engineering
Attn S. Temkin
PO Box 909
Piscataway, NJ 08854

National Oceanic & Atmospheric Adm
Environmental Research Labs
Attn Library, R-51, Tech Rpts
Boulder, CA 80302

Oak Ridge National Laboratory
Attn R. G. Haire
Oak Ridge, TN 37839

Science Applications, International Corp
Attn T. Allik
1710 Goodridge Drive
McLean, VA 22102

Shwartz Electro-Optic, Inc.
Attn G. A. Rines
45 Winthrop Street
Concord, MA 01742

W. J. Schafer Assoc
Attn J. W. Collins
321 Billerica Road
Chelmsford, MA 01824

Union Carbide Corp
Attn M. R. Kokta
50 South 32nd Street
Washougal, WA 98671

Arizona State University
Dept of Chemistry
Attn L Eyring
Tempe, AZ 85281

University of Southern California
Attn M. Birnbaum
Denney Research Bldg., University Park
Los Angeles, CA 90089

DISTRIBUTION (cont'd)

Carnegie Mellon University
Schenley Park
Attn Physics & EE, J. O. Artman
Pittsburgh, PA 15213

Colorado State University
Physics Department
Attn S. Kern
Ft Collins, CO 80523

University of Connecticut
Department of Physics
Attn R. H. Bartram
Storrs, CT 06269

University of South Florida
Physics Dept
Attn R. Chang
Attn Sengupta
Tampa, FL 33620

Howard University
Physics Department
Attn Prof. V. Kushamaha
25 Bryant St., N.W.
Washington, DC 20059

Johns Hopkins University
Dept of Physics
Attn B. R. Judd
Baltimore, MD 21218

Kalamazoo College
Dept of Physics
Attn K. Rajnak
Kalamazoo, MI 49007

Massachusetts Institute of Technology
Crystal Physics Laboratory
Attn H. P. Jenssen
Attn A. Linz
Cambridge, MA 02139

University of Minnesota, Duluth
Department of Chemistry
Attn L. C. Thompson
Duluth, MN 55812

Oklahoma State University
Dept of Physics
Attn R. C. Powell
Stillwater, OK 74078

Pennsylvania State University
Materials Research Laboratory
Attn W. B. White
University Park, PA 16802

Princeton University
Department of Chemistry
Attn D. S. McClure
Princeton, NJ 08544

San Jose State University
Department of Physics
Attn J. B. Gruber
San Jose, CA 95192

Seton Hall University
Chemistry Department
Attn H. Brittain
South Orange, NJ 07099

University of Virginia
Dept of Chemistry
Attn F. S. Richardson (2 copies)
Charlottesville, VA 22901

University of Wisconsin
Chemistry Department
Attn J. Wright
Attn B. Tissue
Madison, WI 53706

Mark Koch
13040 Bennystone
Farmers Branch, TX 75244

US Army Laboratory Command
Attn AMSLC-TD, Technical Director

Installation Support Activity
Attn SLCIS-CC, Legal Office

USAISC
Attn AMSLC-IM-VA, Admin Ser Br
Attn AMSLC-IM-VP, Tech Pub Br (2 copies)

Harry Diamond Laboratories
Attn Division Directors
Attn SLCHD-TL (3 copies)
Attn SLCHD-TL (Woodbridge)
Attn SLCHD-NW-CS, Chief
Attn SLCHD-NW-E, Chief

DISTRIBUTION (cont'd)

Harry Diamond Laboratories (cont'd)
Attn SLCHD-NW-EH, Chief
Attn SLCHD-NW-EP, Chief
Attn SLCHD-NW-ES, Chief
Attn SLCHD-NW-P, Chief
Attn SLCHD-NW-R, Chief
Attn SLCHD-NW-RP, Chief
Attn SLCHD-NW-RS, Chief
Attn SLCHD-NW-TN, Chief
Attn SLCHD-NW-TS, Chief
Attn SLCHD-PO, Chief
Attn SLCHD-ST-C, Chief
Attn SLCHD-ST-RP, Chief
Attn SLCHD-ST-RS, Chief
Attn SLCHD-TT, Chief
Attn SLCHD-TA-ET, B. Willis
Attn SLCHD-TA-ET, B. Zabludowski
Attn SLCHD-NW-EP, C. S. Kenyon
Attn SLCHD-NW-EP, J. R. Miletta
Attn SLCHD-NW-RP, F. B. McLean
Attn SLCHD-NW-RS, L. Libelo
Attn SLCHD-ST-SP, A. A. Bencivenga

Harry Diamond Laboratories (cont'd)
Attn SLCHD-CS, J. Sattler
Attn SLCHD-ST-CB, J. Nemarich
Attn SLCHD-ST-CB, B. Weber
Attn SLCHD-ST-AP, T. Bahder
Attn SLCHD-ST-AP, J. Bradshaw
Attn SLCHD-ST-AP, J. Bruno
Attn SLCHD-ST-AP, E. Harris
Attn SLCHD-ST-AP, R. Leavitt
Attn SLCHD-ST-AP, J. Pham
Attn SLCHD-ST-AP, G. Simonis
Attn SLCHD-ST-AP, M. Stead
Attn SLCHD-ST-AP, J. Stellato
Attn SLCHD-ST-AP, S. Stevens
Attn SLCHD-ST-AP, R. Tober
Attn SLCHD-ST-AP, M. Tobin
Attn SLCHD-ST-AP, G. Turner (10 copies)
Attn SLCHD-ST-AP, D. Wortman
Attn SLCHD-ST-SS, C. Garvin
Attn SLCHD-ST-OP, J. Goff
Attn SLCHD-ST-AP, C. Morrison (10 copies)